Chapter

Assessing Ventilation Strategies to Reduce the Spread of Pathogens in Restaurants

Sanika Bhagwat, Vedant Joshi and Francine Battaglia

Abstract

Since first recognizing COVID-19 as a rapidly spreading virus, research has been pursued to determine how to reduce or mitigate the transmission. Many restaurants reduced capacity and increased distance between tables to maintain social distancing. However, patrons remove masks while eating and this does not guarantee the prevention of viral transmission. The goal of this study was to understand how virus spreads in an air-conditioned restaurant using computational fluid dynamics. Three configurations for supply and return vents were modeled in a scenario where a carrier sneezes and releases virus-laden saliva droplets into the air. The distributions of droplets airborne, deposited on surfaces and exhausted through return vents, were compared to determine where vent configuration reduces the risk of infection for patrons. The effect of air changes per hour (ACH) was studied by comparing the percentages of airborne and exhausted droplets. Lastly, two vent configurations were compared in a scenario with multiple diners talking within the span of 2 minutes. A staggered supply vent configuration was found to be most effective in removing airborne particles. Increasing ACH decreased the percentage of airborne particles. Smaller respiratory particles released by activities like talking have a higher percentage being exhausted than larger sneeze droplets.

Keywords: aerosols, airflow, CFD, respiration, ventilation, viral transmission

1. Introduction

The COVID-19 disease caused by the novel SARS-CoV-2 coronavirus has resulted in infections worldwide and has been classified as a pandemic. Coronavirus is a large family of viruses known to cause respiratory infections in humans and animals. These can range from mild common colds to more severe diseases. COVID-19 first appeared in December 2019 and due to person-to-person transmission, has spread worldwide [1]. According to John Hopkins Coronavirus Resource Center [2], there have been over 645 million known COVID-19 cases as of November 2022. Symptoms of COVID-19 include fever or chills, cough, nasal congestion, shortness of breath, headaches and body aches.

The spread of SARS-CoV-2 is reported to be mainly due to respiratory droplets, air-borne particles and close contact. Respiratory droplets are released due to activities like coughing, sneezing, talking and even breathing. Use of face masks, face shields and maintaining a distance of 6 ft or more from each other are recommended by the Center for Disease Control (CDC) guidelines to limit the spread of this disease. Other methods include washing hands with soap and water and use of alcohol-based hand sanitizers [3].

Since first recognizing COVID-19 as a novel, rapidly spreading virus, significant research has been pursued to study the possible ways of infection and methods of prevention. Karia et al. [4] detail the different modes of COVID-19 transmission. It has been determined that COVID-19 can spread via methods like secretions of body fluids, airborne transmission and fomites (contaminated surfaces). However, the highest risk of transmission is through airborne respiratory particles like aerosols and droplets. Liu et al. [5] studied aerosol transmission, measuring the concentration of SARS-CoV-2 RNA amongst the aerosols sampled from the air in COVID-19 patient wards and other areas frequented by patients and medical staff in two hospitals in Wuhan, China. The study showed that concentration of virus RNA was lower in ventilated patient wards but higher in bathrooms and other crowded areas.

As there are plenty of diseases that spread via airborne droplets, such as influenza and common cold, various studies were conducted to measure the quantity and size distribution of saliva droplets released during human respiratory activities. In one of the earliest experiments, Duguid et al. [6] measured droplets released during coughing, talking and sneezing using direct micrometry from droplet nuclei settled on oiled slides. More recently, a similar experiment was conducted by Xie et al. [7] using glass slides and a microscope to measure the size and number of droplets released due to respiratory activities. They also measured the total mass of droplets released with the help of surgical masks and plastic bags. The study gave the diameter distribution for droplets released during coughing and talking by averaging results for five people coughing 20 times and talking. Wilson et al. [8] measured the total number and volume of aerosols exhaled during breathing, talking, shouting and coughing and therapies such as high-flow nasal oxygen. The study showed that respiratory activities that mimic respiratory patterns during illness generate substantially more aerosols than non-invasive respiratory therapies, which conversely can reduce total emissions. In another study by Leonard et al. [9], the authors demonstrated the efficacy of surgical masks in reducing particulate transmission.

Apart from experiments, studies using numerical methods and computational fluid dynamics (CFD) to model particles released during respiratory activities have been conducted to analyze the spread of COVID-19. Wei and Li [10] studied the effect of turbulence and evaporation on dispersion of droplets in a cough jet using a discrete random walk model. In presence of velocity fluctuations, small droplets were dispersed in the whole jet region, of which 1% of large droplets (100 mm) were transported over 2 m. Small droplets (30 mm) were not sensitive to relative humidity (RH) and became droplet nuclei soon after being expired, and then behaved similarly as small particles. Medium droplets were very sensitive to humid conditions (RH above 80%), as they settled but deposited slowly, and therefore were carried forward in the jet-induced velocity field. Zhu et al. [11] used CFD to study transport characteristics of saliva droplets in an indoor space. They showed that for smaller droplets (30 μm), inertia and gravity do not play a significant role and droplets were carried along with the airflow. For droplets 50 μm–200 μm, gravity was significant and they fell as the airflow weakened, whereas, larger droplets (300 μm), traveled farther due

to inertia. Yan et al. [12] studied the thermal effect of the human body on evaporation and dispersion of cough droplets. An Eulerian-Lagrangian coupling approach was used to model the cough droplets released from a body with and without heat transfer. It was found that the thermal effect did not cause a significant change in the evaporation rate of droplets. But it affected the deposition time of smaller droplets (0.35 μm–20 μm) that were trapped in the ascending thermal flow and stayed in air longer.

Zhang et al. [13] conducted experimental and CFD analyses of virus transmission in a university campus bus. The study showed 2 m distance was not enough to prevent virus transmission due to turbulent airflow caused by the HVAC system. On the other hand, the turbulence mixed the aerosols with the ambient air thereby reducing concentration. Opening the doors and windows reduced the aerosol concentration by half. The use of transparent barriers to mitigate the spread of aerosols was investigated by Abuhegazy et al. [14] for a classroom and Joshi and Battaglia [15] to assess infection risk of musicians in an orchestra. Liu et al. [16] recreated a scenario of a restaurant in China where an asymptomatic COVID-19 patient led to the infection of eight people seated at the same and adjacent tables. This simulation used an in-house large eddy simulation (LES) solver with Eulerian-Lagrangian coupling. The regions of aerosol exposure in the simulation corresponded to the reported pattern of infection in the restaurant.

Most indoor restaurants have a ventilation system to maintain thermal comfort and air quality for patrons and employees. Clean air is introduced in the room through the supply vents while room air is exhausted through the return vents and sent to the air conditioning system. Ventilation strategies for maintaining thermal comfort were studied by Joshi et al. [17]. The rate of change of air in the room is important for maintaining acceptable air quality. ASHRAE standard 62.1 [18] recommends an air flow rate of 7.5 cfm per person or 0.18 cfm/ft.^{2} for restaurant dining rooms.

Eating at restaurants is an important part of our social lives. Many restaurants have reduced capacity and increased distance between tables to maintain social distancing during the pandemic. However, patrons remove masks while eating and this may not guarantee the prevention of COVID-19 transmission. Respiratory droplets from infected carriers may be inhaled by other people or deposit on food at other tables, potentially spreading infection. These respiratory droplets can be entrained in the moving air. In closed-space air-conditioned restaurants, the position of air vents and direction of air flow plays an important role in risk of infection for the patrons as evident by the study conducted by Liu et al. [16] on COVID-19 transmission in a restaurant in Guangzhou, China.

While there are plenty of studies that use CFD to analyze COVID-19 transmission, few are focused specifically on restaurants, despite having a large influence on the spread of the virus. This study aims to incorporate CFD to model saliva droplets released through various respiratory activities in a restaurant scenario. Ventilation strategies, including vent locations and air flow rates, will be examined to determine ways to reduce infection risk. Respiratory activities like sneezing and talking will be studied in order to determine if a distance of 2 m between restaurant tables is sufficient to reduce virus transmission.

2. Restaurant configurations

The restaurant dining area modeled in this study is a rectangular room with a 13 m length, 6 m width, and 3.5 m height. There are seven tables arranged in two rows with

four patrons at each table, and a reception desk with a receptionist. The patrons and receptionist are modeled as cuboids of 1 m height and 0.35 m length and width (representing people in a seated position). The layout of the restaurant is shown in **Figure 1** with the COVID-19 carrier marked with red. There are 16 vents with 12 on the ceiling and 4 on the wall opposite to the row with the COVID-19 carrier. The vents on the ceiling are each 0.6 m × 0.6 m and the vents on the wall are each 0.4 m × 0.8 m. At a given time, four of these vents act as supply vents and four act as return vents. The vent configurations are given in the **Figure 2**. The first configuration has supply and return vents on the ceiling and the supply vents are parallel to the return vents. The supply vents are in a straight line above the tables on one side of the room (above the COVID-19 carrier). The return vents are in a straight line above the opposite row of tables. The second configuration also has both supply and return vents on the ceiling but the return vents are in a straight line in the center of the room, and the supply vents are staggered on both sides of the return vents. In the third configuration, the return vents are on the ceiling above the row of tables on the side of the COVID-19 carrier. The supply vents in this case are on the opposite wall but parallel to the return vents.

The ambient temperature of the room initially is 25°C and the constant supply of air introduced through the vents is at 21°C. Each ceiling vent is divided into four and

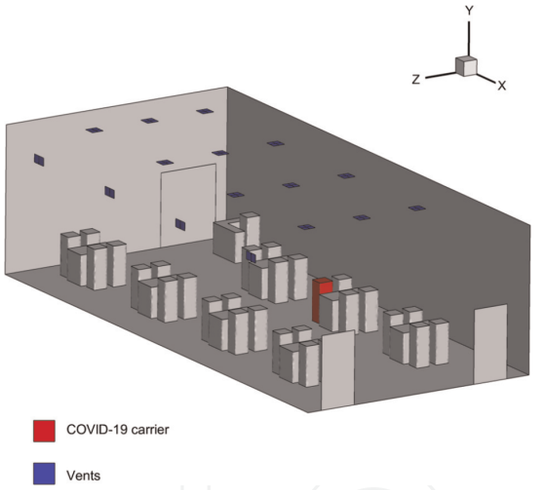

Figure 1.
Restaurant configuration with 4 patrons per table showing ceiling and wall vents.

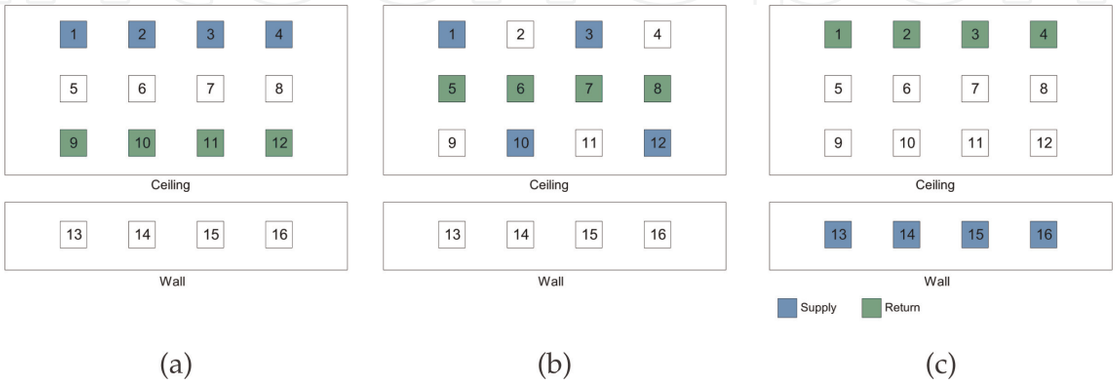

Figure 2.
Vent configurations (a) ceiling (S parallel), (b) ceiling (S staggered), and (c) ceiling/wall (S parallel). Blue represents supply vents and green represents return vents.

air flows through them at a 30° angle from the ceiling in four directions. Each wall vent is divided into two and air flows through them at 30° from the horizontal and 45° from the wall in two opposite directions. The patrons are modeled with a heat flux of 1224.5 kW from their top surface to represent heat release from their head.

3. Numerical methodologies

The CFD software ANSYS Fluent [19] is used to solve the Reynolds-Averaged Navier-Stokes (RANS) flow equations for the conservation of mass and momentum. The continuity equation is:

$$\frac{\partial \rho}{\partial t} + \vec{\nabla} \cdot \left(\rho \vec{V}\right) = 0 \tag{1}$$

where t is time, ρ is density and $\overleftarrow{V}$ is the velocity vector.
The governing equations for conservation of momentum are:

$$\frac{\partial \left(\rho \vec{V}\right)}{\partial t} + \rho \vec{V}\left(\vec{\nabla} \cdot \vec{V}\right) = -\vec{\nabla} p + \vec{\nabla} \cdot \bar{\bar{\tau}} + \rho \vec{g} \tag{2}$$

where p is pressure,$\bar{\bar{\tau}}$ is fluid stress tensor and $\vec{g}$ is gravitational body force.
The energy equation is:

$$\frac{\partial}{\partial t}(\rho E) + \vec{\nabla} \cdot \left[\vec{V}(\rho E + p)\right] = \vec{\nabla} \cdot k_{eff} \vec{\nabla} T + \vec{\nabla} \cdot \left(\bar{\bar{\tau}}_{eff} . \vec{V}\right) \tag{3}$$

where E is total energy and k_{eff} is effective conductivity for the total fluid thermal conductivity and turbulent thermal conductivity.

The realizable k-ε turbulence model was employed in this study, which contains a formulation for the turbulent viscosity for better predictions for the flows involving boundary layers in strong adverse pressure gradients, separation and re-circulation zones. The transport equations for turbulence kinetic energy k and turbulence dissipation ε are:

$$\frac{\partial}{\partial t}(\rho k) + \vec{\nabla} \cdot \left(\rho k \vec{V}\right) = \vec{\nabla} \cdot \left[\left(\mu + \frac{\mu_t}{\sigma_\varepsilon}\right) \vec{\nabla} k\right] + G_k + G_b - \rho \varepsilon \tag{4}$$

and

$$\frac{\partial}{\partial t}(\rho \varepsilon) + \vec{\nabla} \cdot \left(\rho \varepsilon \vec{V}\right) = \vec{\nabla} \cdot \left[\left(\mu + \frac{\mu_t}{\sigma_\varepsilon}\right) \vec{\nabla} \varepsilon\right] - \rho C_2 \frac{\varepsilon^2}{k + \sqrt{\nu \varepsilon}} + C_{1\varepsilon} \frac{\varepsilon}{k} C_{3\varepsilon} G_b \tag{5}$$

where μ is molecular viscosity of the fluid, μ_t is the turbulence viscosity, G_k is the generation of turbulent kinetic energy due to mean velocity gradients and G_b is the generation of turbulent kinetic energy due to buoyancy. The constants are $C_{1\varepsilon} = 1.44$, $C_2 = 1.9$, $\sigma_\varepsilon = 1.2$, and $\sigma_k = 1.0$. The constant $C_{3\varepsilon}$ determines the degree to which turbulence dissipation ε is affected by buoyancy and is calculated using the flow velocity component parallel and perpendicular to the gravitational vector.

The release of respiration particles uses the discrete phase model in ANSYS Fluent. The model employs an Euler-Lagrange approach where the fluid flow in the continuous phase is solved using the Navier-Stokes equations, while trajectory of the particles is predicted by:

$$\frac{du_p}{dt} = F_D\left(u - u_p\right) + g\frac{\left(\rho_p - \rho\right)}{\rho_p} \tag{6}$$

where u is the fluid phase velocity, u_p is particle velocity, $F_D\left(u - u_p\right)$ is the drag force per unit particle mass:

$$F_D = \frac{18\mu}{\rho_p {d_p}^2}\frac{C_D\, Re}{24} \tag{7}$$

where ρ_p is density of the particle and d_p is particle diameter. The Reynolds number for the particle motion is:

$$Re = \frac{\rho d_p |u_p - u|}{\mu} \tag{8}$$

The pressure-based Navier-Stokes (PBNS) solver is used in this study. The pressure and velocity are coupled using the semi-implicit method for pressure-linked equation (SIMPLE) algorithm. The least squares cell based and PRESTO! schemes are used to discretize gradient and pressure, respectively. Momentum is discretized using the QUICK scheme, and second-order upwind is used to discretize the energy, turbulent kinetic energy and dissipation rates.

The time step, Δt for the simulations was selected such that the Courant-Fredrichs-Levy (CFL) number is close to one:

$$CFL = V\frac{\Delta t}{\Delta x} \tag{9}$$

where V is the inlet velocity and Δx is the cell size. A grid resolution study was performed, as detailed in **Appendix A**, to estimate error and accuracy of the mesh.

4. Results

4.1 Vent configurations during sneezing

Of all respiratory activities, sneezing is the most explosive and releases a large number of droplets with a high velocity. Droplets are carried over large distances and are one of the primary ways of spreading infection for airborne diseases like COVID-19. The simulation of sneeze particles in air is used to analyze infection risk associated with different vent configurations. Other respiratory activities such as talking and breathing at rest are suitable to study with the CFD modeling presented in Section 3. For a restaurant scenario, talking will be considered in Subsection 4.3 talking as a secondary source that could spread a virus.

In the first part of the study, the COVID-19 carrier is seated in the restaurant at table (refer to **Figure 1**). The person sneezes across the table at an angle 30° downwards. The sneeze consists of 18,000 particles of which 2000 particles are classified as aerosols (0.5 μm–5 μm) and 16,000 particles as droplets (5 μm–150 μm). The diameter distribution for the particles was the same as that reported by Xie et al. [7]. A 5-minute flow simulation was completed with the ventilation turned on (ACH = 6) but without introducing particles to allow airflow in the restaurant to reach a quasi-steady state. This was used as the initial condition for the simulation with the sneeze particles for another 5 minutes. The sneeze particles were introduced at 14 s of this simulation. The sneeze lasted for 0.5 s with 1800 particles introduced every time step (Δt = 0.05 s).

The sneeze particles carried by the airflow in the room were either exhausted through the return vents or deposit on various surfaces in the room. Some particles deposit on adjacent tables and can potentially infect the people eating food placed on these tables. Also, any particle that remains airborne can pose a risk of infection for the restaurant patrons and staff. In 5 minutes, most of the sneeze particles are either exhausted or deposited. This is demonstrated in **Figure 3** which shows the time history for percentage of airborne particles. By the end of 5 minutes less than 10% particles are left airborne. This shows that 5 minutes is sufficient time to study the deposition of particles in the room.

The dispersion of particles throughout the room for the three vent configurations is shown in the **Figure 4**. Most of the particle dispersion took place within the first 2 minutes hence, smaller time intervals are chosen within the first three rows compared to the last two to get a better understanding of activity in the room. The first row (**Figure 4a**) shows sneeze particles after 20 s. There is not much difference between the vent configurations at this time. Sneeze particles rise up in a plume above the COVID-19 carrier. At 30 s (**Figure 4b**), sneeze particles have started to disperse horizontally for the Ceiling (S parallel) and the Ceiling (S staggered) cases but still stay in a vertical column for the Ceiling/Wall (S parallel) case due to the return vent being right above the table in the Ceiling/Wall (S parallel) case. At 60 s (**Figure 4c**), in the Ceiling (S parallel) and the Ceiling (S staggered) cases, sneeze particles are

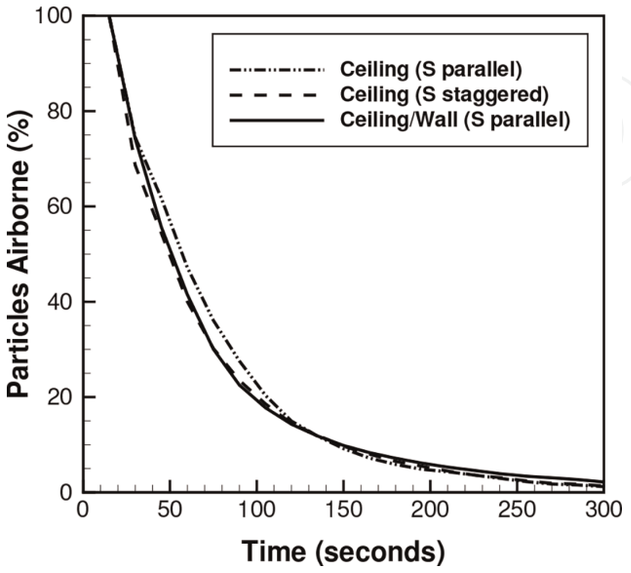

Figure 3.
Time history of airborne particles for ceiling (S parallel), ceiling (S staggered) and ceiling/wall (S parallel) vent configurations.

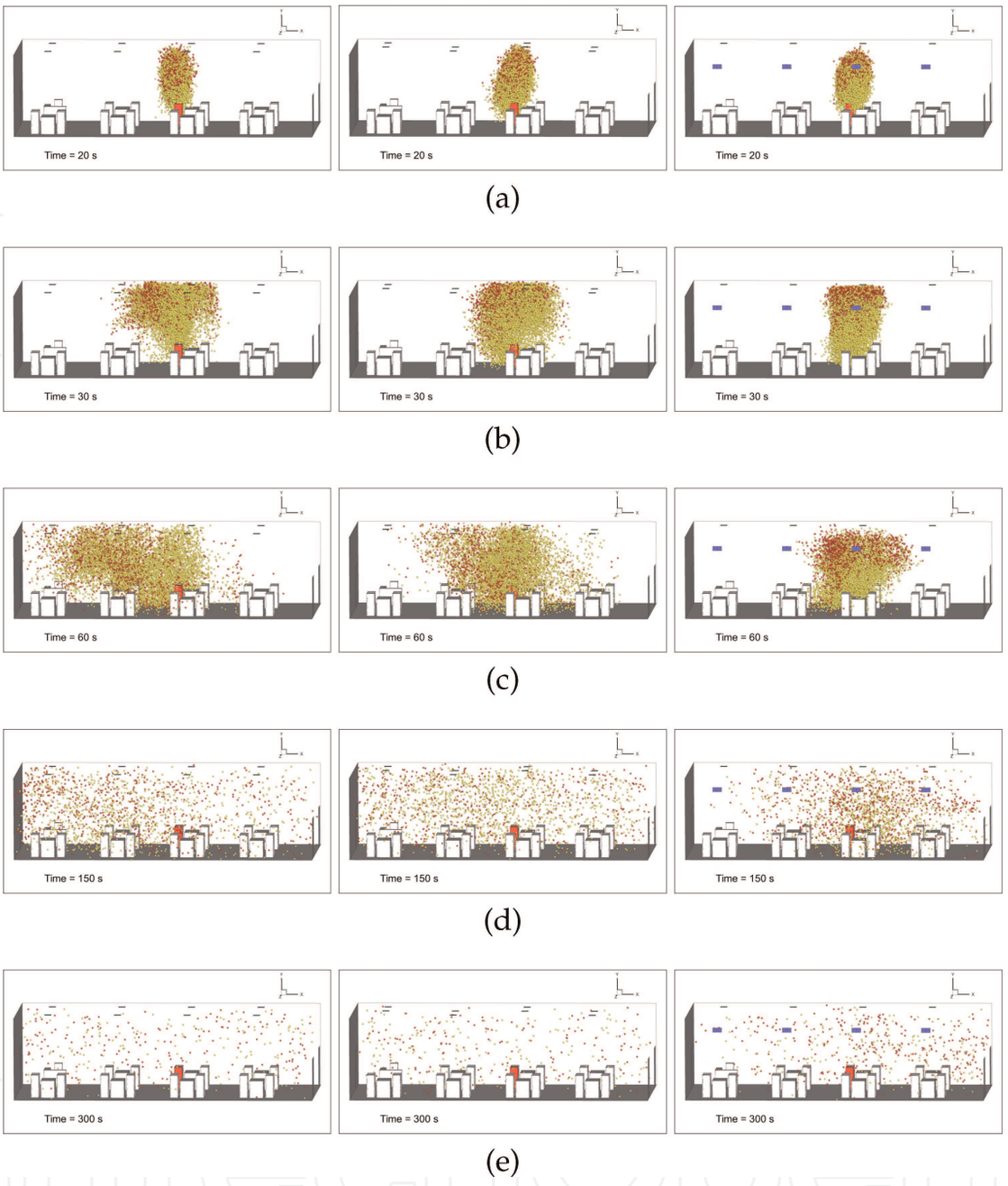

Figure 4.
Comparison of sneeze particle dispersion for ceiling (S parallel) (first column), ceiling (S staggered) (middle column) and ceiling/wall (S parallel) (third column) for (a) t = 20 s, (b) t = 30 s, (c) t = 60 s, (d) t = 150 s, and (e) t = 300 s. Red color represents aerosols and yellow represents droplets.

carried backwards by the airflow from the supply vent above the patron and in the Ceiling/Wall (S parallel) case they are carried forward by the sneeze velocity. The sneeze particles have traveled farthest for the Ceiling (S parallel) case and are still relatively close to the patron in the Ceiling/Wall (S parallel) case. By 150 s (**Figure 4d**), the sneeze particles have dispersed all over the room for all three vent configurations but the concentration of particles is still highest near the patron in the Ceiling/Wall (S parallel) case. By the end of 5 minutes (**Figure 4e**), very few particles remain airborne. The number of airborne particles is highest for the Ceiling/Wall (S parallel) case.

Vent configuration	Aerosols exhausted (%)	Droplets exhausted (%)
Ceiling (S parallel)	4.85	2.05
Ceiling (S staggered)	10.95	5.93
Ceiling/wall (S parallel)	16.35	4.68

Table 1.
Percentage of exhausted aerosols and droplets.

Table 1 shows a comparison of the percentage of aerosols and droplets individually exhausted to the return vents. The initial sneeze was modeled with 11.1% aerosols and 88.9% droplets. The percentage of aerosols exhausted is significantly higher than the percentage of droplets exhausted for all cases. This may be due to the fact that aerosols are lighter and tend to rise up and get carried by the airflow through the return vents. Droplets being heavier are not easily affected by the airflow and settle. Since the sneeze consists of a majority of droplets, a large percentage of the total number of particles are deposited on the floor while the percentage of particles exhausted is low.

Figure 5 shows the percentage of particles exhausted through each vent. For the Ceiling (S parallel) configuration, the particles exhausted through each vent are evenly distributed. But for the other two configurations, most of the particles are exhausted through only one vent. This vent happens to be the one closest to the COVID-19 carrier, indicating that for the Ceiling (S parallel) configuration, the particles disperse through the entire room.

4.2 Increasing air changes per hour

The recommended number of air changes per hour (ACH) for restaurants is 6–12 to maintain adequate supply of fresh air necessary for the health of the occupants [18]. The results presented in Subsection 4.1 were for simulations when 6 ACH was maintained for each ventilation strategy. To understand the effect of ACH on the spread of particles in the room, in this section, three values of ACH are studied. The setup for this study is similar to Subsection 4.1 with regards to the location of the COVID-19 carrier and the sneeze particles. The Ceiling (S staggered) vent configuration was chosen as the reference case. ACH values of 6, 9 and 12 were maintained by changing the inlet velocity. The use of high-efficiency particulate air (HEPA) filters would slightly alter the ACH but is not considered explicitly as the three cases cover a wide range of possible values. The inlet velocities for 6, 9 and 12 ACH are 2.77 m/s, 4.15 m/s and 5.54 m/s, respectively. The dispersion of particles at the end of 5 minutes was compared.

The dispersion of particles are presented in **Figure 6** for 9 and 12 ACH respectively. These are compared to 6 ACH shown in **Figure 4** (middle column). At 20 s, not much difference can be observed between 6 ACH (**Figure 4a**, middle column) and 9 ACH (6 (a), first column), but for 12 ACH (**Figure 6a**, second column), sneeze particles are dispersed backwards due to the higher inlet velocity. At 30 s, compared to 6 ACH (**Figure 4b**, middle column), the sneeze particles have dispersed more in the 9 ACH and 12 ACH cases (**Figure 6b**). This trend continues in the next 30 s as shown in **Figure 4c**, middle column; and **Figure 6c**. In the 12 ACH case, a majority of the sneeze particles have traveled behind the sneezing patron. By 150 s (**Figure 4d**, middle column; and **Figure 6d**), sneeze particles

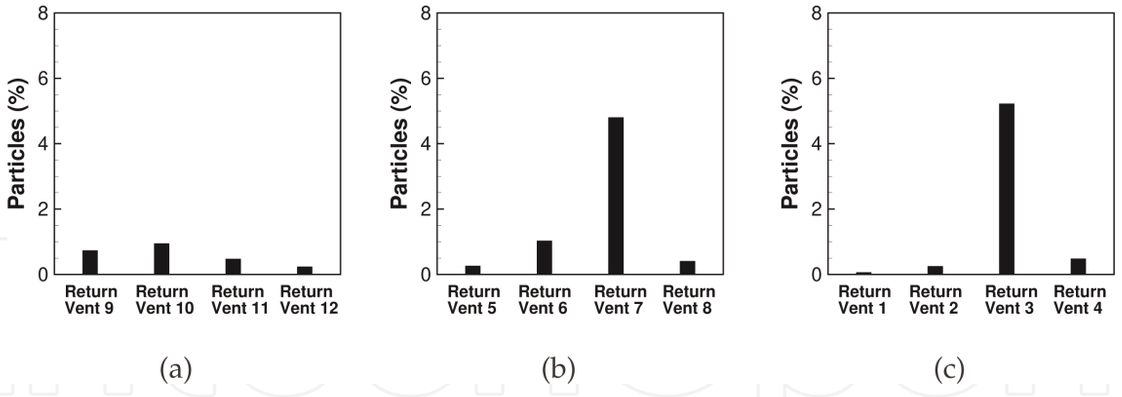

Figure 5.
Percentage of sneeze particles exhausted through each vent configuration: (a) ceiling (S parallel), (b) ceiling (S staggered), and (c) ceiling/wall (S parallel).

have dispersed throughout the room. For the 9 ACH and 12 ACH cases, majority of the particles have been carried behind the patron due to higher inlet velocity from the supply vent above the patron. At 300 s, most of the particles have either been exhausted to the return vents or deposited on various surfaces. Very few particles are still airborne. The number of airborne particles are highest in the 6 ACH case and lowest in the 12 ACH case (**Figure 4e**, middle column; and **Figure 6e**).

Figure 7 shows the trend of airborne and exhausted particles with increasing ACH. The percentage of exhausted particles is highest for 9 ACH (8.81%) but decreases to 3.27% for 12 ACH. The higher downward velocity for 12 ACH pushes the particles towards the floor which is why the percentage of exhausted particles is lower and a larger number of particles are deposited on the floor. As the percentage of exhausted particles first increases for 9 ACH and then decreases for 12 ACH, increasing ACH may not result in a higher success in removing virus from the room. On the other hand, percentage of airborne particles decreases with increasing ACH, posing lower infection risk for the occupants.

4.3 Talking

The previous scenarios investigated one COVID-19 carrier at a fixed location. However, in a restaurant there are multiple people who release respiratory particles regularly due to various activities like talking and breathing. In this section, two vent configurations are compared for a scenario involving multiple people talking. **Figure 8** shows the people who talk within the duration of the simulation marked in red. Simulations for the Ceiling (S parallel) and Ceiling (S staggered) cases are compared for multiple people talking for 5 minutes. The first instance of talking occurs at 5 s and all people finish talking by 2 minutes, with each person talking twice. During the rest of the simulation, the talking particles are dispersed throughout the room. The particles released during talking range from 0.1μm to 10 μm [6]. Each person released 40 particles during each second of talking. The people talking are chosen at random but at least one person is talking within an interval of 10 s.

The dispersion of talking particles in the room for the Ceiling (S parallel) and the Ceiling (S staggered) cases are shown in **Figure 9**. The people can be seen talking between 5 s and 120 s. At 15 s (**Figure 9a**), talking are particles released by the first two people seated at table-4. Since the first person talks in the forward direction,

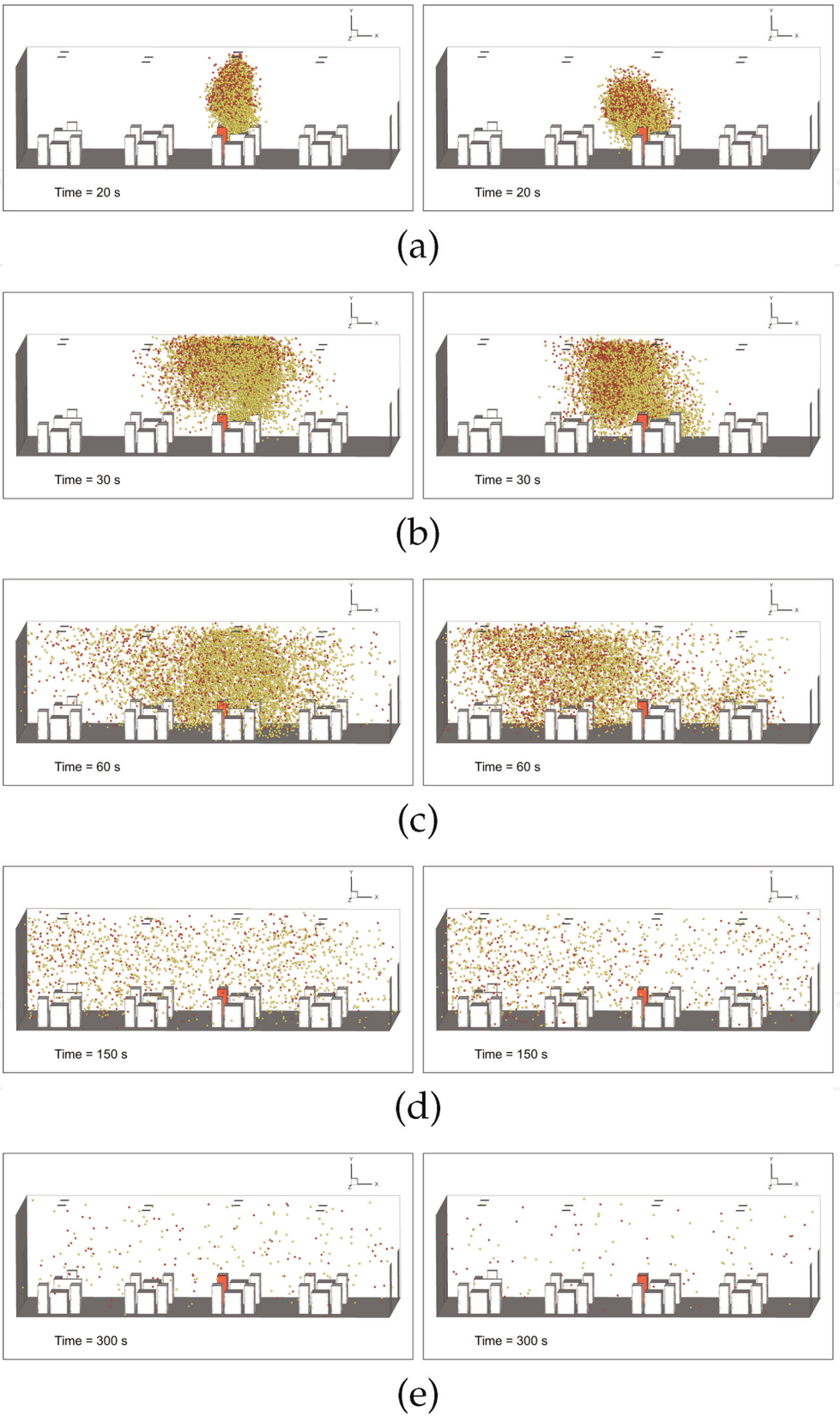

Figure 6.
Comparison of sneeze particle dispersion for 9 ACH (first column) and 12 ACH (second column) at (a) t = 20 s, (b) t = 30 s, (c) t = 60 s, (d) t = 150 s, and (e) t = 300 s. Red represents aerosols and yellow represents droplets.

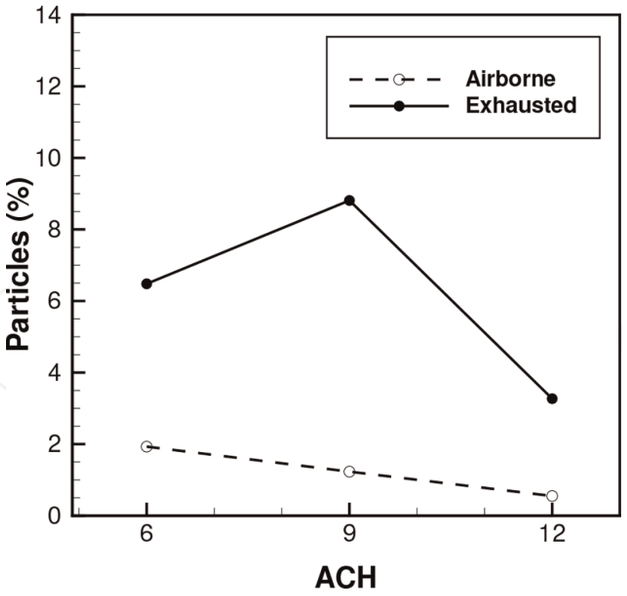

Figure 7.
Airborne and exhausted particles versus ACH.

particles are carried forward by talking velocity in the Ceiling (S parallel) case but in the Ceiling (S staggered) case, forward motion of the particles is disrupted due to the air velocity from the supply vent above. By 45 s (**Figure 9b**), talking particles released by multiple people are dispersed throughout the room. A higher concentration of particles are near the person talking at table-1 (1d). Due to staggered vents, particles are more dispersed in the Ceiling (S staggered) case compared to the Ceiling (S parallel) case. By 75 s (**Figure 9c**), all 10 people have talked at least once and most twice. The talking particles are dispersed throughout room. There is not much difference between the two vent configurations. In the last two rows (**Figure 9d** and **e**), since there are not people talking anymore, the concentration of particles in the room decreases with time as they are exhausted or deposited.

In the sneeze scenario in Subsection 4.1, the exhausted particles were evenly distributed throughout the return vents for the Ceiling (S parallel) configuration and the same is the case for talking particles (**Figure 10**). For the Ceiling (S staggered)

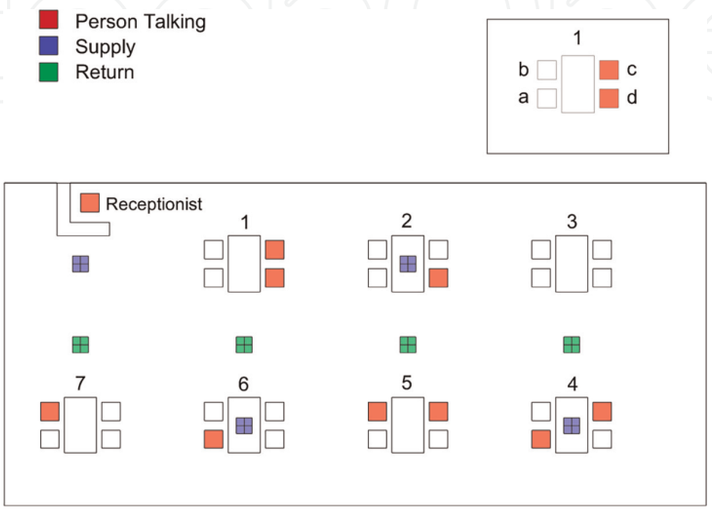

Figure 8.
Top view of locations for people talking. Supply and return vent on the ceiling are identified.

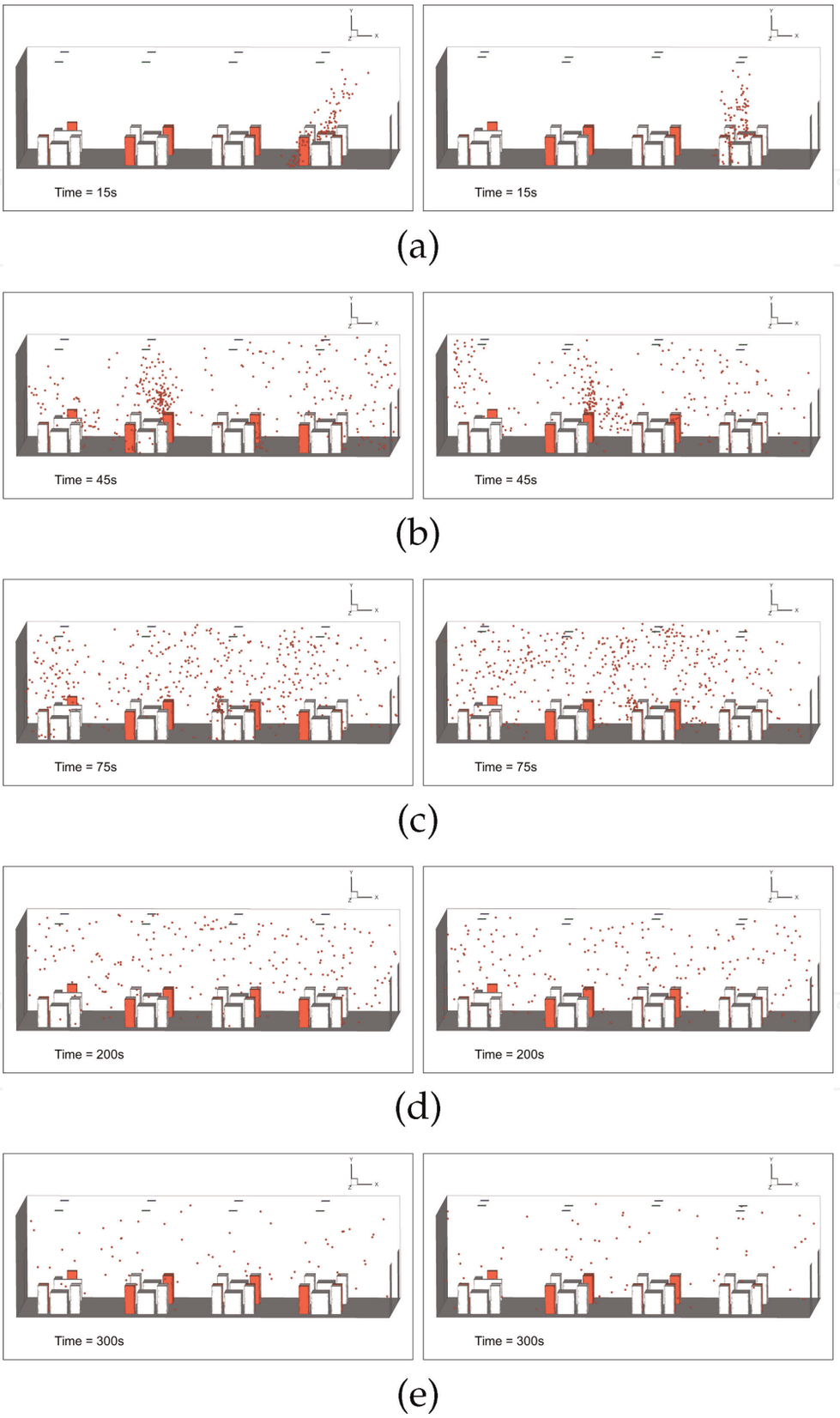

Figure 9.
Comparison of dispersion of talking particles for ceiling (S parallel) (first column) and ceiling (S staggered) (second column) for (a) t = 15 s, (b) t = 45 s, (c) t = 75 s, (d) t = 200 s, and (e) t = 300 s.

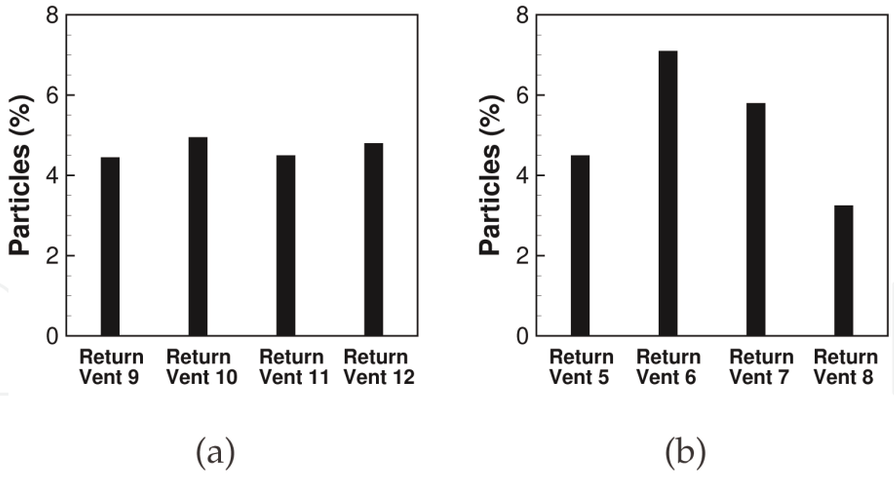

Figure 10.
Percentage of talking particles exhausted through each vent: (a) ceiling (S parallel), and (b) ceiling (S staggered).

case, while most sneeze particles were exhausted through only one vent, for talking, particles are more evenly distributed as the people releasing the particles are spread out across the room.

5. Conclusions

A scenario with a virus-infected patron sneezing in a restaurant was modeled and three vent configurations were compared. The first two configurations had supply and return vents on the ceiling and one configuration had supply vents parallel to the return vents and the other with staggered supply vents. The third configuration had supply vents on the wall. It was found that the percentage of airborne particles was lowest for the staggered supply configuration. The percentage of exhausted particles was also highest for the staggered supply configuration. Hence, the staggered supply vent configuration was considered as the one with least risk of virus transmission. The effect of increasing air changes per hour was studied by comparing 6, 9 and 12 ACH for the staggered supply configuration. The percentage of airborne particles reduced with increasing ACH.

A scenario with multiple restaurant patrons talking was also modeled. A comparison of the parallel and staggered ceiling supply configurations with talking showed that percentage of airborne particles was similar in both cases but the percentage of exhausted particles was higher in the staggered supply case. This supports the argument that the staggered supply vent configuration is the safest. A summary of the results is given in **Table 2**. Talking particles larger than 5 μm are considered as aerosols as they are smaller than most droplets and behave similar to aerosols.

It was found that aerosols (0.5 μm–5 μm) being lighter, rise and were carried by the airflow and droplets (5 μm–150 μm) being heavier were not affected much by the airflow and settled. Sneeze particles consist of a majority of droplets. Hence, most of the sneeze particles were deposited on the floor and not more than 10% were exhausted. Very few sneeze particles were deposited on the adjacent tables (placed 2 m apart). On the other hand, talking particles mostly consist of aerosols. The percentage of exhausted particles in the talking scenario (about 20%) was higher than the sneeze scenario. In case of talking, a 2 m distance between tables may not be sufficient.

Case		Airborne (%)		Exhausted (%)		Deposited (%)	
		Aerosol	Droplet	Aerosol	Droplet	Aerosol	Droplet
Sneeze	Ceiling (S parallel)	1.09	0.95	1.22	5.27	8.84	82.47
	Ceiling (S staggered)	0.89	1.04	1.82	4.67	8.40	83.18
	Ceiling/Wall (S parallel)	1.67	1.27	0.54	1.83	8.91	85.79
ACH	6 ACH	0.89	1.04	1.82	4.67	8.40	83.18
	9 ACH	0.47	0.77	2.12	6.64	8.47	81.48
	12 ACH	0.26	0.29	1.52	1.80	9.33	86.79
Talk	Ceiling (S parallel)	5.63	N/A	18.79	N/A	75.58	N/A
	Ceiling (S staggered)	5.71	N/A	20.67	N/A	73.62	N/A

Table 2.
Summary of particles airborne, exhausted and deposited for sneezing, ACH and talking cases.

Appendix A

A grid resolution study was performed to get an estimate of the error and accuracy of the results. A grid convergence index (GCI) study was conducted using three meshes described in **Table 3**. The geometry modeling and meshing was created using Ansys ICEM. Tetrahedral meshes created in ICEM were converted to polyhedral meshes in Ansys Fluent [19]. The geometry used is the same as that of the restaurant shown in **Figure 1**. The Ceiling (S parallel) vent configuration was simulated for 6 air changes per hour, where ACH refers to the number of times the entire volume of air in the room is replaced by supply air. The COVID-19 carrier sneezes at 14 s after the start of the simulation and the percentages of sneeze particles airborne at the end of 60 s were compared for the three meshes. The time-averaged velocity and temperature profiles for three positions in the room are analyzed and **Figure 11** shows the locations. **Figure 12** shows the temperature profiles and **Figure 13** shows the velocity profiles at the three positions for the three meshes. GCI calculated using the percentage of airborne particles is given in **Table 4**. The fine, medium and coarse mesh are associated with numbers 1, 2, and 3, respectively, and GCI_{21} refers to the error between the fine and medium mesh and GCI_{32} refers to the error between the medium and coarse mesh. The procedure for this is detailed in Celik et al. [20]. The mesh size, h is given by:

$$h = \left[\frac{1}{N}\sum_{i=1}^{N}(\Delta V_i)\right]^{1/3} \tag{10}$$

Mesh	Fine (1)	Medium (2)	Coarse (3)
Mesh size (h)	0.025 m	0.05 m	0.1 m
Number of cells	4,818,451	747,146	115,852
CPU (days)	5	2	1

Table 3.
Mesh resolution details.

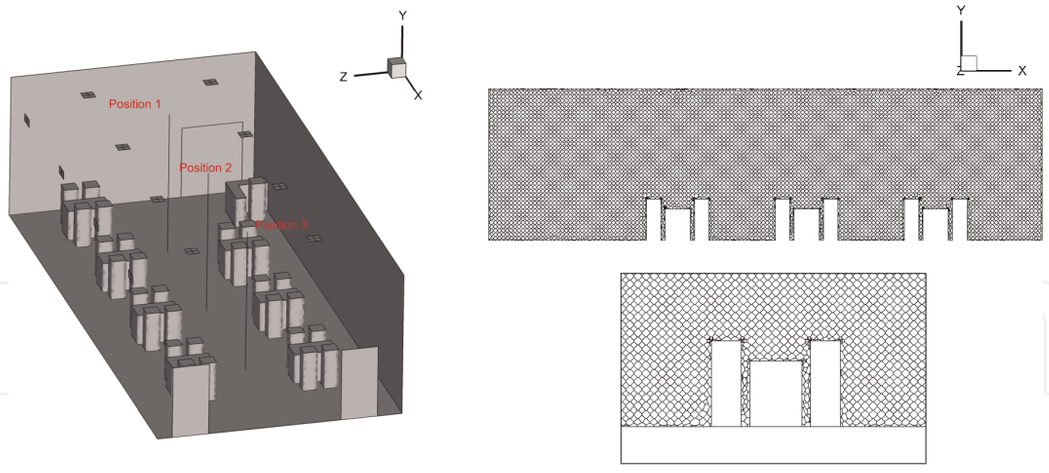

Figure 11.
(a) Positions where velocity and temperature profiles are compared, and (b) medium mesh sample.

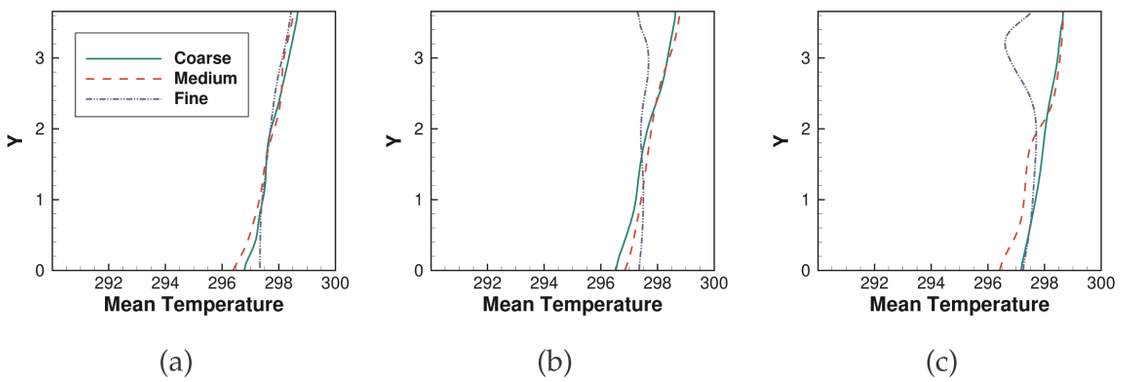

Figure 12.
Temperature profiles at (a) position 1, (b) position 2, and (c) position 3 for coarse (green, solid line), medium (red, dashed line), and fine (blue, dash dot dot line) mesh.

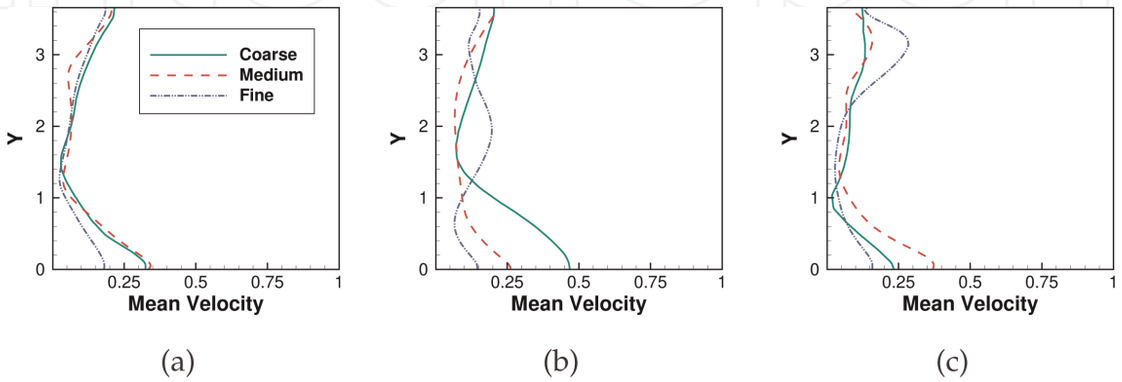

Figure 13.
Velocity profiles at (a) position 1, (b) position 2, and (c) position 3 for coarse (green, solid line), medium (red, dashed line), and fine (blue, dash dot dot line) mesh.

Parameter	Airborne particles (%)
Fine (1)	23.78
Medium (2)	25.98
Coarse (3)	37.05
GCI_{21}	2.62
GCI_{32}	9.24

Table 4.
Percentage of airborne particles.

where N is the total number of cells and ΔV_i is the volume of the i^{th} cell.

The error in the percentage of particles is less than 10% as shown in **Table 4**. While there is some difference between the medium and fine meshes as seen from the velocity and temperature profiles (**Figures 12** and **13**), the computational time for fine mesh is very large. Hence, the medium mesh was selected for the study.

Author details

Sanika Bhagwat, Vedant Joshi and Francine Battaglia*
The Department of Mechanical and Aerospace Engineering, University at Buffalo, The State University of New York, Buffalo, NY, USA

*Address all correspondence to: fbattagl@buffalo.edu

References

[1] Center for Disease Control and Prevention. About COVID-19. 2019. Available from: https://www.cdc.gov/coronavirus/2019-ncov/your-health/about-covid-19.html

[2] Johns Hopkins University and Medicine. Johns Hopkins Coronavirus Resource Center. 2022. Available from: https://coronavirus.jhu.edu/

[3] Center for Disease Control and Prevention. How Covid Spreads. 2019. Available from: https://www.cdc.gov/coronavirus/2019-ncov/prevent-getting-sick/how-covid-spreads.html

[4] Karia R, Gupta I, Khandait H. COVID-19 and its modes of transmission. SN Comprehensive Clinical Medicine. 2020;**2**:1798-1801. DOI: 10.1007/s42399-020-00498-4

[5] Liu Y, Ning Z, Chen Y. Aerodynamic analysis of SARS-CoV-2 in two Wuhan hospitals. Nature. 2020;**582**:557-560. DOI: 10.1038/s41586-020-2271-3

[6] Duguid JP. The size and the duration of air-carriage of respiratory droplets and droplet-nuclei. Epidemiology and Infection. 1946;**44**(6):471-479. DOI: 10.1017/S0022172400019288

[7] Xie X, Li Y, Sun H, Liu L. Exhaled droplets due to talking and coughing. Journal of the Royal Society Interface. 2009;**6**:S703-S714. DOI: 10.1098/rsif.2009.0388.focus

[8] Wilson N, Corbett S, Tovey E. Airborne transmission of COVID-19. BMJ. 2020;**370**:m3206. DOI: 10.1136/bmj.m3206

[9] Leonard S, Strasser W, Whittle JS, Volakis LI, DeBellis RJ, Prichard R, et al. Reducing aerosol dispersion by high flow therapy in COVID-19: High resolution computational fluid dynamics simulations of particle behavior during high velocity nasal insufflation with a Simple surgical mask. Journal of the American College of Emergency Physicians Open. 2020;**1**(4):578-591. DOI: 10.1002/emp2.12158

[10] Wei J, Li Y. Enhanced spread of expiratory droplets by turbulence in a cough jet. Building and Environment. 2015;**93**:86-96. DOI: 10.1016/j.buildenv.2015.06.018

[11] Zhu S, Kato S, Yang JH. Study on transport characteristics of saliva droplets produced by coughing in a calm indoor environment. Building and Environment. 2006;**41**:1691-1702. DOI: 10.1016/j.buildenv.2005.06.024

[12] Yan Y, Li X, Tu J. Thermal effect of human body on cough droplets evaporation and dispersion in an enclosed space. Building and Environment. 2019;**148**:96-106. DOI: 10.1016/j.buildenv.2018.10.039

[13] Zhang Z, Han T, Yoo KH, Capecelatro J, Boehman AL, Maki K. Disease transmission through expiratory aerosols on an urban bus. Physics of Fluids. 2021;**33**:015116. DOI: 10.1063/5.0037452

[14] Abuhegazy M, Talaat K, Anderoglu O, Poroseva SV. Numerical investigation of aerosol transport in a classroom with relevance to COVID-19. Physics of Fluids. 2020;**32**:103311. DOI: 10.1063/5.0029118

[15] Joshi V, Battaglia F. A risk assessment of pathogen transport during an indoor orchestra performance. In: Proceedings of the ASME 2021 International Mechanical Engineering

Congress and Exposition. Volume 10: Fluids Engineering. Virtual, Online. New York: ASME; 2021. V010T10A006. DOI: 10.1115/IMECE2021-73290

[16] Liu H, He S, Shen L, Hong J. Simulation-based study of COVID-19 outbreak associated with air-conditioning in a restaurant. Physics of Fluids. 2021;**33**:023301. DOI: 10.1063/5.0040188

[17] Jazizadeh F, Joshi V, Battaglia F. Adaptive and distributed operation of HVAC systems: Energy and comfort implications of active diffusers as new adaptation capacities. Building and Environment. 2020;**186**:107089. DOI: 10.1016/j.buildenv.2020.107089

[18] ASHRAE. ASHRAE Standard 62.1-2019, Ventilation for Acceptable Indoor Air Quality. Atlanta, GA: ASHRAE; 2019

[19] ANSYS. Fluent Theory Guide Release. Vol. 19. Canonsburg, PA: ANSYS Inc.; 2019

[20] Celik IB et al. Procedure for estimation and reporting of uncertainty due to discretization in CFD applications. Journal of Fluids Engineering-Transactions of the ASME. 2008;**130**(7):078001. DOI: 10.1115/1.2960953